

# Novel Foxo1-dependent transcriptional programs control Treg cell function



Published in final edited form as:
*Nature*. 2012 November 22; 491(7425): 554–559. doi:10.1038/nature11581.

# Novel Foxo1–dependent transcriptional programs control $T_{reg}$ cell function

**Weiming Ouyang**[1], **Will Liao**[2,3], **Chong T. Luo**[1,4], **Na Yin**[1], **Morgan Huse**[1], **Myoungjoo V. Kim**[1], **Min Peng**[1], **Pamela Chan**[1], **Qian Ma**[1], **Yifan Mo**[2,3], **Dies Meijer**[5], **Keji Zhao**[6], **Alexander Y. Rudensky**[1,7], **Gurinder Atwal**[2], **Michael Q. Zhang**[8,9], and **Ming O. Li**[1]

[1]Immunology Program, Memorial Sloan-Kettering Cancer Center, New York, New York 10065, USA [2]Cold Spring Harbor Laboratory, Cold Spring Harbor, New York 11724, USA [3]Department of Applied Mathematics & Statistics, Stony Brook University, Stony Brook, New York 11794, USA [4]Louis V. Gerstner, Jr Graduate School of Biomedical Sciences, Memorial Sloan-Kettering Cancer Center, New York, New York 10065, USA [5]Department of Cell Biology and Genetics, Erasmus University Medical Center, 3000 DR Rotterdam, The Netherlands [6]Systems Biology Center, NHLBI, National Institute of Health, Bethesda, Maryland 20892, USA [7]Howard Hughes Medical Institute, Memorial Sloan-Kettering Cancer Center, New York, New York 10065, USA [8]Department of Molecular and Cell Biology, Center for Systems Biology, The University of Texas at Dallas, Richardson, Texas 75080, USA [9]Bioinformatics Division, Center for Synthetic and Systems Biology, TNLIST, Tsinghua University, Beijing 100084, China

## Abstract

Regulatory T ($T_{reg}$) cells, characterized by expression of the transcription factor forkhead box P3 (Foxp3), maintain immune homeostasis by suppressing self-destructive immune responses[1–4]. Foxp3 operates as a late-acting differentiation factor controlling $T_{reg}$ cell homeostasis and function[5], whereas the early $T_{reg}$-cell-lineage commitment is regulated by the Akt kinase and the forkhead box O (Foxo) family of transcription factors[6–10]. However, whether Foxo proteins act beyond the $T_{reg}$-cell-commitment stage to control $T_{reg}$ cell homeostasis and function remains largely unexplored. Here we show that Foxo1 is a pivotal regulatorof $T_{reg}$ cell function. $T_{reg}$ cells express high amounts of Foxo1 and display reduced T-cell-receptor-induced Akt activation, Foxo1 phosphorylation and Foxo1 nuclear exclusion. Mice with $T_{reg}$-cell-specific deletion of *Foxo1* develop a fatal inflammatory disorder similar in severity to that seen in Foxp3-deficient mice, but without the loss of $T_{reg}$ cells. Genome-wide analysis of Foxo1 binding sites reveals ~300 Foxo1-bound target genes, including the pro-inflammatory cytokine *Ifng*, that do not seem to be directly regulated by Foxp3. These findings show that the evolutionarily ancient Akt–Foxo1 signalling module controls a novel genetic program indispensable for $T_{reg}$ cell function.



Correspondence and requests for materials should be addressed to M.O.L. (lim@mskcc.org) or M.Q.Z. (mzhang@cshl.edu) for computational questions..

**Supplementary Information** is available in the online version of the paper.

**Author Contributions** W.O., W.L., C.T.L., N.Y., M.H., G.A., M.Q.Z. and M.O.L. designed the research and analysed the data; W.O., W.L., C.T.L., N.Y., M.H., M.V.K., M.P., P.C., Q.M. and Y.M. did the experiments; D.M. and A.Y.R. provided *birA* and *Foxp3*$^{cre}$ mouse strains; K.Z. supervised the ChIP-seq experiment; and W.O., W.L. and M.O.L. wrote the manuscript.

**Author Information** The expression and ChIP-seq data have been deposited in the NCBI GEO database under accession number GSE40657. Reprints and permissions information is available at www.nature.com/reprints.

The authors declare no competing financial interests. Readers are welcome to comment on the online version of the paper.

Among the three *Foxo* genes expressed in T cells, the transcript of *Foxo1* is specifically upregulated in mature thymocytes[8]. To genetically mark cells expressing Foxo1, we engineered a *Foxo1* allele (*Foxo1*$^{tag}$) encoding an in-frame fusion protein tag containing green fluorescent protein (GFP), Flag and a biotin-labelling peptide that enables Foxo1 biotinylation in *birA*-transgenic mice that express the bacterial biotin ligase BirA (Fig. 1a and Supplementary Fig. 1). T-cell expression of CD127 (also known as Il7r), the product of a previously identified Foxo1 target gene[11,12], was unaffected in *Foxo1*$^{tag/tag}$ mice (Supplementary Fig. 1d), indicating that the protein tag does not alter Foxo1 function. Using GFP as a reporter, we found that immature thymocytes expressed low amounts of Foxo1 (Fig. 1a). Foxo1 was more strongly upregulated in $T_{reg}$ cells than in conventional CD4$^+$ T cells in the thymus, whereas the peripheral T cells expressed similar amounts of Foxo1 (Fig. 1a).

Foxo1 resides in the nucleus of quiescent T cells, and relocates to the cytosol after T-cell receptor (TCR) stimulation. To investigate the kinetics of Foxo1 translocation, we performed live-imaging experiments on CD4$^+$ T cells from *Foxo1*$^{tag/tag}$ mice on a *Foxp3*-internal ribosome entry site (*IRES*)-red fluorescent protein (*RFP*)-transgenic background in which $T_{reg}$ cells are marked by the expression of RFP. Whereas high-dose CD3 antibody induced Foxo1 nuclear clearance in all T cells (Fig. 1b, c and Supplementary Video 1), low-dose CD3 antibody triggered Foxo1 translocation in conventional T cells but not in $T_{reg}$ cells (Fig. 1b, c and Supplementary Video 2). Attenuated Foxo1 nuclear clearance in $T_{reg}$ cells was further revealed by the immunostaining of T cells from wild-type mice (Supplementary Fig. 2a, b). Foxo1 nuclear export is regulated by Akt-induced Foxo1 phosphorylation. Low-dose anti-CD3 induced robust Akt and Foxo1 phosphorylation in conventionalT cells, which was markedly decreased in $T_{reg}$ cells (Fig. 1d). The phosphorylation defects of Foxo1 and Akt were less profound in T cells stimulated with high-dose CD3 antibody (Supplementary Fig. 2c). Anti-CD3-induced Erk1 and Erk2 (also known as Mapk3 and Mapk1, respectively) phosphorylation was not compromised at the late time points in $T_{reg}$ cells (Fig. 1d and Supplementary Fig. 2c), suggesting that the Akt pathway might be specifically modulated, probably through high expression of the Akt phosphatase Phlpp1 (ref. 13). Thus, compared to conventional T cells, $T_{reg}$ cells are resistant to TCR-induced Akt activation and Foxo1 nuclear clearance.

To investigate the function of Foxo1 in $T_{reg}$ cells, we crossed mice carrying floxed *Foxo1* alleles (*Foxo1*$^{fl/fl}$) with *Foxp3*$^{cre}$ mice[14]. Foxo1 protein was barely detectable in $T_{reg}$ cells from *Foxp3*$^{cre}$ *Foxo1*$^{fl/fl}$ mice, whereas conventional CD4$^+$ T cells from *Foxp3*$^{cre}$ *Foxo1*$^{fl/fl}$ mice expressed comparable amounts of Foxo1 to wild-type T cells (Fig. 2a). In the absence of Foxo1 in $T_{reg}$ cells, mice developed a hunched posture associated with lack of mobility, in addition to crusting of the ears, eyelids and tail (Fig. 2b) before they became moribund within 35 days of birth. Such a fulminant phenotype was comparable in severity to that of mice with the scurfy mutation of the *Foxp3* gene (*Foxp3*$^{sf}$; Fig. 2b), or mice depleted of $T_{reg}$ cells[15,16]. In addition, *Foxp3*$^{cre}$ *Foxo1*$^{fl/fl}$ mice showed splenomegaly and lymphadenopathy (Fig. 2c), and had a dense infiltrate of leukocytes in the salivary glands, lung interstitia, liver sinusoids, pancreas acini, stomach, and colon mucosa (Fig. 2d).

The severe immunopathology was associated with the expansion of T-cell populations expressing high amounts of the cell-proliferation marker Ki67 (Fig. 2e and Supplementary Fig. 3). T cells displayed an effector/memory phenotype (Fig. 2f and Supplementary Fig. 4a) and produced increased amounts of the pro-inflammatory cytokine interferon (IFN)-γ (Fig. 2g and supplementary Fig. 4b). Deletion of *Foxo1* from CD4$^+$CD8$^+$ immature T cells results in compromised $T_{reg}$ cell differentiation[8,10]. However, thymic and splenic $T_{reg}$ cell numbers were unaffected in 12-day-old *Foxp3*$^{cre}$ *Foxo1*$^{fl/fl}$ mice (Supplementary Fig. 5). By the age of day 20, $T_{reg}$ cell numbers in the peripheral lymphoid tissues were increased in

*Foxp3*$^{cre}$ *Foxo1*$^{fl/fl}$ mice (Fig. 2h and Supplementary Fig. 4c). These findings imply that the lymphoproliferative disease is caused by a loss of $T_{reg}$ cell function rather than a loss of $T_{reg}$ cells.

The observation that $T_{reg}$ cells were less sensitive to TCR-induced Foxo1 nuclear exclusion implies that Foxo1-dependent transcriptional regulation is crucial for $T_{reg}$ cell function. However, cytosolic Foxo1 regulates autophagy through transcription-independent mechanisms[17]. To differentiate the activities of nuclear Foxo1 and cytosolic Foxo1 induced by Akt activation, we inserted a complementary DNA fragment coding for a haemagglutinin (HA)-tagged human Foxo1 mutant in which amino acids at the Akt phosphorylation sites were substituted with alanines[18] (HA-hFoxo1(AAA)), preceded by a *loxP*-flanked `*neo*-STOP' cassette into the *Rosa26* locus (Supplementary Fig. 6). Mice carrying the mutant allele (*Foxo1*$^{AAA}$) were crossed with oestrogen receptor-Cre (*creER*) mice. Wild-type T cells or T cells from *creER Foxo1*$^{AAA/+}$ mice previously treated with tamoxifen to induce HA-hFoxo1(AAA) expression were stimulated with CD3 and CD28 antibodies. As expected, whereas wild-type Foxo1 translocated from the nucleus to the cytosol, the HA-hFoxo1(AAA)-expressing mutant was defective in nuclear export (Supplementary Fig. 6c). We further crossed *Foxo1*$^{AAA/+}$ mice with *Foxp3*$^{cre}$ mice, and confirmed specific HA-hFoxo1(AAA) expression in $T_{reg}$ cells (Fig. 3a). Ectopic expression of HA-hFoxo1(AAA) did not affect $T_{reg}$ cell differentiation or homeostasis (Supplementary Fig. 7a). Upon breeding the *Foxo1*$^{AAA}$ allele to *Foxp3*$^{cre}$ *Foxo1*$^{fl/fl}$ mice, the lethal inflammatory phenotype was completely rescued (Fig. 3b and supplementary Fig. 7), indicating that the $T_{reg}$ cell defects are caused by a loss of nuclear Foxo1 activity.

For global identification of Foxo1 DNA-binding sites in $T_{reg}$ cells, we performed chromatin immunoprecipitation coupled to high-throughput sequencing (ChIP-seq) experiments using Foxo1 antibody precipitation of chromatin purified from $CD4^+CD25^+$ T cells from C57BL/6 mice, or streptavidin pull-down of chromatin from $T_{reg}$ cells of *Foxo1*$^{tag/tag}$ *birA* mice. To define a ChIP-seq peak as significant, we used the model-based analysis of ChIP-seq (MACS) peak calling software and applied an empirical false-discovery rate of 0.01 at which the noise ratio of peak detection was less than 0.005 (Supplementary Fig. 8a). Using this criterion, we identified 3,431 enriched genomic loci that were shared between the antibody and the biotinylated Foxo1 samples (Supplementary Fig. 8b), and were designated as putative Foxo1 binding sites (Supplementary Table 1). Among the Foxo1binding peaks, we could identify previously characterized binding sites of Foxo1 target genes, including an intronic binding site in the *Foxp3* locus[8], an *Il7r* enhancer element[11,12], as well as binding sites in the proximal promoter regions of the *Fbxo32* and *Bcl2l11* genes[19,20] (Supplementary Fig. 9).

Foxo1 binding sites were mostly enriched in the promoters and the 5′ untranslated regions (UTRs), whereas peaks mapped to the intergenic regions and 3′ UTRs were substantially under-represented (Fig. 3c). Further analysis of the peaks showed that Foxo1 preferentially bound to regions within 500 base pairs of the transcription start sites (Supplementary Fig. 8c). Foxo1 binding peaks were enriched for the high-affinity Foxo1 binding motifs, and *de novo* motif prediction from the top 500 ranked binding peaks revealed a conserved Foxo1 recognition site (Supplementary Fig. 8d, e). In addition, approximately 73% of Foxo1 binding sites were mapped to the conserved genomic regions of mammalian species (Supplementary Table 1). These observations support an evolutionarily conserved function for Foxo1 in classical transcriptional regulation of target-gene expression.

To identify the cellular functions directly regulated by Foxo1 transcriptional control, we performed gene-expression profiling on $T_{reg}$ cells from wild-type, *Foxp3*$^{cre}$*Foxo1*$^{fl/fl}$, *Foxp3*$^{cre}$*Foxo1*$^{AAA/+}$ and *Foxp3*$^{cre}$*Foxo1*$^{fl/fl}$ *Foxo1*$^{AAA/+}$ mice. Comparison of data from

wild-type and *Foxp3*$^{cre}$*Foxo1*$^{fl/fl}$ $T_{reg}$ cells revealed 942 and 1,155 genes downregulated or upregulated, respectively, by more than 1.5 fold, ~80% of which were corrected in *Foxp3*$^{cre}$*Foxo1*$^{fl/fl}$ *Foxo1*$^{AAA/+}$ $T_{reg}$ cells (Supplementary Table 2). By cross-referencing this data set with the data set of Foxo1-bound genes, we identified 310 putative Foxo1 direct target genes, among which 240 and 70 genes were activated or repressed, respectively, by Foxo1 (Fig. 3d and Supplementary Table 3).

$T_{reg}$ cell homeostasis and function are dependent on the $T_{reg}$-cell-specific transcription factor Foxp3 (ref. 5). ChIP and genome tiling array studies have revealed Foxp3-bound genes in murine T cells[21,22]. Approximately 6.8% or 9.6% of Foxo1-bound genes were occupied by Foxp3 in $T_{reg}$ cells or in a T-cell line that overexpressed Foxp3 (Supplementary Fig. 10a). Comparison of the putative direct target genes of Foxo1 and Foxp3 revealed that ~90% of activated genes and ~99% of repressed genes were specifically regulated by Foxo1 or Foxp3 (Supplementary Fig. 10b, c and Supplementary Table 3). Indeed, expression of the Foxp3 target gene *Il2ra* (coding for CD25) was decreased in T cells transcribing a *Foxp3* null allele that encodes a GFP reporter[23], but not in Foxo1-deficient $T_{reg}$ cells (Fig. 4a and Supplementary Fig. 10d). A recent study showed that Foxo1 binds to the promoter region of the Foxp3 target gene *Ctla4* (ref. 10). ChIP-seq experiments revealed weak *Ctla4*-promoter binding of Foxo1 in antibody but not biotin samples (data not shown). In the absence of Foxo1, CTLA4 was marginally downregulated, whereas the amount of *Ctla4* transcript was approximately fourfold lower in the absence of Foxp3 (Fig. 4a and Supplementary Fig. 10e). Foxp3 and CTLA4 are essential for $T_{reg}$ cell inhibition of conventional T-cell proliferation in vitro[23,24]. By contrast, as previously reported in ref. 11, Foxo1-deficient $T_{reg}$ cells had normal suppressive activity in such assays (Fig. 4b). These observations imply that the Foxp3-dependent program is largely intact in the absence of Foxo1, and the loss of suppressive activity of Foxo1-deficient $T_{reg}$ cells is probably independent of CTLA4.

To gain insights into the general functional features of the Foxo1-regulated program, we analysed the Gene Ontology and BioCarta pathway association of Foxo1 target genes[25]. The putative Foxo1 direct target genes were strongly associated with cell communication, signal transduction, transcription and metabolism, and were specifically enriched for genes involved in the Jak-STAT, TCR and insulin-signalling pathways (Supplementary Table 4). A salient characteristic of $T_{reg}$ cells is their inability to produce pro-inflammatory cytokines such as IFN-γ. Foxo1 was recruited to a regulatory element located 22 kilobases upstream from the transcriptional start site of the *Ifng* gene[26] in $T_{reg}$ cells (Fig. 4c, d). In the absence of Foxo1, IFN-γ messenger RNA and protein were highly induced in $T_{reg}$ cells (Fig. 4e, f and Supplementary Fig. 11a). However, similar to wild-type $T_{reg}$ cells, Foxo1-deficient $T_{reg}$ cells were unable to produce interleukin (IL)-2 (Supplementary Fig. 11b), which is probably regulated by Foxp3 (ref. 22). To determine whether Foxo1 had a cell-intrinsic role in inhibiting IFN-γ expression, we co-cultured wild-type $T_{reg}$ cells and $T_{reg}$ cells from the disease-free *creER Foxo1*$^{fl/fl}$ mice previously treated with tamoxifen to acutely delete *Foxo1*. A sizable fraction of Foxo1-deficient but not wild-type $T_{reg}$ cells produced IFN-γ under the condition of IL-12 and IFN-γ stimulation (Supplementary Fig.12a). Importantly, wild-type and Foxo1-deficient conventional $CD4^+$ T cells produced similar amounts of IFN-γ (Supplementary Fig. 12b), revealing a specific function for Foxo1 in repressing IFN-γ expression in $T_{reg}$ cells.

To investigate whether IFN-γ production by Foxo1-deficient $T_{reg}$ cells contributed to their loss of suppressive function, we crossed *Foxp3*$^{cre}$*Foxo1*$^{fl/fl}$ mice to the IFN-γ-deficient background. Ablation of IFN-γ partially corrected the lethal inflammatory phenotype as well as the lymphoproliferative disease of *Foxp3*$^{cre}$*Foxo1*$^{fl/fl}$ mice (Supplementary Fig. 13). To assess the specific function of IFN-γ produced by Foxo1-deficient $T_{reg}$ cells, we used a transfer model of colitis. Recipient mice deficient in recombination-activating gene 1

(*Rag1*$^{-/-}$) did not develop colitis upon receipt of wild-type, *Foxo1*$^{-/-}$ or *Foxo1*$^{-/-}$ *Ifng*$^{-/-}$ $T_{reg}$ cells (Supplementary Fig. 14). However, recipients of naive T cells developed a wasting disease and colitis within 4 weeks, which was prevented by wild-type but not Foxo1-deficient $T_{reg}$ cells (Fig. 4g, h and Supplementary Fig. 14b). Importantly, the suppressive activity was largely restored in *Foxo1*$^{-/-}$ *Ifng*$^{-/-}$ $T_{reg}$ cells (Fig. 4g, h and Supplementary Fig. 14b), supporting *Ifng* as a critical Foxo1 target gene in the control of $T_{reg}$ cell function.

Foxo proteins control Foxp3 expression and $T_{reg}$ cell differentiation[8–10]. Our new data reveal that the Akt–Foxo1 signalling pathway is modulated in mature $T_{reg}$ cells to maintain high nuclear Foxo1 activity; this is crucial for $T_{reg}$ cell function, in part through Foxo1 inhibition of IFN-γ expression. IFN-γ produced by $T_{reg}$ cells may activate conventional T cells or antigen-presenting cells compromising $T_{reg}$ cell function, but the precise mechanisms remain to be determined. Diminished TCR-induced Akt activation has been observed in human $T_{reg}$ cells[27], suggesting that Foxo1 controls human $T_{reg}$ cell function. Under conditions of strong TCR stimulation, nuclear Foxo1 is translocated to the cytosol in $T_{reg}$ cells, raising the possibility that the Foxo1-dependent program is subject to regulation. Intriguingly, $T_{reg}$ cells from mice infected with *Toxoplasma gondii* produce IFN-γ[28]. Increased frequencies of IFN-γ-secreting $T_{reg}$ cells are also present in multiple sclerosis and diabetes patients[29,30]. Future studies will determine whether the loss of Foxo1 function accounts for $T_{reg}$ cell plasticity under these pathological conditions, and whether the Akt–Foxo1 signalling pathway can be manipulated for the treatment of $T_{reg}$-cell-associated immunological disorders.

## METHODS

### Mice

To generate a *Foxo1* knock-in mouse model (*Foxo1*$^{tag}$), two genomic DNA fragments of the *Foxo1* gene were isolated from a C57BL/6 bacterial artificial chromosome library (Genome Systems). A cDNA coding for GFP, Flag and biotin-labelling peptide was inserted into the genomic DNA fragment containing the second exon of *Foxo1* before the stop codon. Targeting vector was constructed by cloning the fragments into pEasy-Flox plasmid. To generate a *Rosa26-hFoxo1*$^{AAA}$ knock-in mouse model (*Foxo1*$^{AAA}$), the cDNA coding for a HA-tagged human Foxo1 (AAA) mutant was inserted into a *Rosa26* targeting vector. Linearized targeting vectors were transfected into embryonic stem cells derived from the C57BL/6 strain. Homologous recombinants were identified by Southern blotting analysis, and were implanted into foster mothers. Chimaeric mice were bred to C57BL/6 mice, and the $F_1$ generation was screened for germline transmission. The *neo* gene in *Foxo1*$^{tag}$ mice was removed by breeding $F_1$ mice with a strain of *cytomegalovirus*-promoter-driven *cre*-transgenic mice (The Jackson Laboratory). Mice containing floxed *Foxo1*, *Foxp3-IRES-RFP*, *Foxp3*$^{Cre}$, *Foxp3*$^{gfpko}$ (*Foxp3* null allele coding for a GFP reporter) and *birA* alleles were previously described[11,14,23,31,32]. C57BL/6, *Foxp3*$^{sf}$, *Ifng*$^{-/-}$, *Rag1*$^{-/-}$ and *UBC-cre-ERT2* (*creER*) mice were purchased from the Jackson Laboratory. Mice with intact or floxed *Foxo1* alleles were used as wild-type controls. Mice with $T_{reg}$-cell-specific deletion of *Foxo1* were generated by crossing *Foxo1* floxed mice with *Foxp3*$^{cre}$ mice. To mark $T_{reg}$ cells with RFP, mice were bred with *Foxp3-IRES-RFP* mice. To label Foxo1 with biotin, *Foxo1*$^{tag}$ mice were bred with *birA*-transgenic mice. All mice were maintained under specific pathogen-free conditions, and animal experimentation was conducted in accordance with institutional guidelines.

### Antibodies and immunoblotting

Anti-p-Foxo1 Thr 24 (no. 9464), anti-Foxo1 (C29H4), anti-p-Akt Ser 473 (D9E), anti-Akt (C67E7), anti-p-Erk1/2, anti-Erk1/2 and anti-HA (6E2) were purchased from Cell Signaling.

Anti-β-actin (AC-15) was obtained from Sigma. To determine Foxo1 expression in $T_{reg}$ cells, $CD4^+Foxp3^+$ $T_{reg}$ cells were purified by FACS. Total protein extracts were dissolved in SDS sample buffer. To assess Foxo1 translocation, T cells were stimulated with anti-CD3 and anti-CD28, and the cytosolic and nuclear extracts were prepared. To analyse Akt, Foxo1 and Erk phosphorylation, conventional $CD4^+$ T cells and $CD4^+Foxp3^+$ $T_{reg}$ cells were purified by FACS. T cells were stimulated with anti-CD3 and anti-CD28, and the total protein extracts were prepared. Protein extracts were separated on 8% SDS–PAGE gels and transferred to polyvinylidene difluoride membrane (Millipore). The membranes were probed with antibodies and visualized with the Immobilon Western Chemiluminescent HRP Substrate (Millipore).

## Live imaging of Foxo1 translocation

$CD4^+$ cells were isolated from *Foxo1*$^{tag/tag}$ *Foxp3-IRES-RFP* mice, and stimulated with plate-bound anti-CD3 and anti-CD28 on glass surfaces. GFP, RFP and bright-field images were acquired every 2 min after addition of cells using a fluorescence videomicroscope (Olympus IX-81) fitted with a 40X objective lens. Nuclear Foxo1 clearance was quantified by analysing two orthogonal linescans through each cell. For each linescan, the average intensity of three equally spaced pixels inside the cell was divided by the average intensity of the cell edge on each side to determine a `clearance ratio'. Nuclear exclusion leads to a decrease in clearance ratio.

## Immunofluorescence microscopy

$CD4^+$ T cells were isolated from spleen and peripheral lymph nodes of C57BL/6 mice with anti-CD4 microbeads (Miltenyi Biotec Inc.), stimulated with plate-bound anti-CD3 (low dose, 0.01 μg $ml^{-1}$; high dose, 0.1 μg $ml^{-1}$) and anti-CD28 (1 μg $ml^{-1}$) on chamber slides at 37 °C for 20 min. After fixation with 4% paraformaldehyde, cells were permeabilized with Foxp3 Fixation/Permeabilization buffer (eBioscience) according to the manufacturer's instructions. After blocking with Permeabilization buffer and 3% BSA, cells were incubated with 1:250 diluted rabbit anti-Foxo1 (C29H4, Cell Signaling) and rat anti-Foxp3 (FJK-16 s, eBioscience), followed by allophycocyanin (APC)-anti-rabbit and fluorescein isothiocyanate (FITC)-anti-rat secondary antibodies in Permeabilization buffer and 1% BSA. Slides were mounted with gold anti-fading mounting buffer (Invitrogen). Images were acquired with a Leica TCS SP5-II confocal microscope. For quantitative analysis, five fields were selected randomly and total cells in the field were manually counted and grouped with Volocity software (PerkinElmer Inc.), on the basis of their Foxo1 nuclear or cytosolic localization and Foxp3 expression.

## Flow cytometry

Fluorescent-dye-labelled antibodies against cell-surface markers CD4, CD8, TCR-β, CD44, CD62L, CTLA4 and CD25 were purchased from eBiosciences. Thymic, splenic and lymph node cells were depleted of erythrocytes by hypotonic lysis. Cells were incubated with specific antibodies for 30 min on ice in the presence of 2.4G2 monoclonal antibody to block FcγR binding. All samples were acquired and analysed with an LSR II flow cytometer (Becton, Dickinson) and FlowJo software (TreeStar). Intracellular Foxp3, CTLA4 and Ki67 stainings were carried out with kits from eBiosciences. To determine cytokine expression, splenic and lymph node T cells were stimulated with 50 ng $ml^{-1}$ phorbol 12-myristate 13-acetate (Sigma), 1 μM ionomycin (Sigma) and GolgiStop (BD Biosciences) for 4 h. After stimulation, cells were stained with cell-surface marker antibodies, fixed and permeabilized, and stained with anti-Foxp3 in combination with specific antibodies against IFN-γ and IL-2 (eBiosciences).

### ELISA

$T_{reg}$ cells were purified from wild-type and *Foxp3*$^{cre}$ *Foxo1*$^{fl/fl}$ mice by FACS and stimulated with CD3 and CD28 antibodies in the presence of IL-2 for 24 h. Cytokine amounts in tissue-culture supernatants were assayed with ELISA antibody pair for IFN-γ (eBioscience, 88-8312) in accordance with the manufacturer's recommendations.

### *In vitro* T-cell differentiation

CreER-mediated deletion of floxed *Foxo1* alleles was induced by intraperitoneal injection of 2 mg of tamoxifen (Sigma) emulsified in 200 ml of corn oil (Sigma) every day for 5 days. $CD4^+Foxp3^+$ $T_{reg}$ cells or $CD44^{lo}CD4^+Foxp3^-$ conventional T cells from $CD45.1^+$ wild-type and $CD45.2^+$ tamoxifen-treated *creER Foxo1*$^{fl/fl}$ (*Foxo1*$^{-/-}$) mice were isolated by FACS and were co-cultured at 1:1 ratio with irradiated splenocytes, anti-CD3 (1 μg ml$^{-1}$), anti-CD28 (2 μg ml$^{-1}$) and IL-2 (200 U ml$^{-1}$) in the presence or absence of IL-12 (5 ng ml$^{-1}$) and IFN-γ (10 ng ml$^{-1}$) for 3 days.

### *In vitro* $T_{reg}$ cell suppression

$CD44^{lo}CD4^+Foxp3^-$ conventional T cells labelled with CFSE were used as responder cells. Responder T cells ($5 \times 10^4$) were cultured for 72 h with irradiated splenocytes ($1 \times 10^5$) and anti-CD3 (2 μg ml$^{-1}$) in the presence or absence of various numbers of $T_{reg}$ cells. The division of responder T cells was assessed by dilution of CFSE.

### Transfer model of colitis

Naive T cells sorted by FACS ($CD4^+CD44^{lo}CD62L^{hi}$, $4 \times 10^5$) from $CD45.1^+$ C57BL/6 mice were transferred into *Rag1*$^{-/-}$ mice alone or in combination with $CD45.2^+$ $T_{reg}$ cells ($CD4^+Foxp3^+$, $2 \times 10^5$). After T-cell reconstitution, mice were weighed weekly and monitored for signs of disease. Mice were killed at 4 weeks after T-cell transfer and their colons were used for histopathological analysis. The following grades were used to evaluate their disease severity: 0, normal colonic crypt architecture; 1, mild inflammation: slight epithelial cell hyperplasia and increased numbers of leukocytes in the mucosa; 2, moderate colitis: pronounced epithelial hyperplasia, significant leukocyte infiltration, and decreased numbers of goblet cells; 3, severe colitis: marked epithelial hyperplasia with extensive leukocyte infiltration, significant depletion of goblet cells, occasional ulceration, or cryptic abscesses; 4, very severe colitis: marked epithelial hyperplasia with extensive transmural leukocyte infiltration, severe depletion of goblet cells, many crypt abscesses and severe ulceration.

### Histopathology

Tissues from killed animals were fixed in Safefix II (Protocol) and embedded in paraffin. 5-μm sections were stained with haematoxylin and eosin.

### ChIP-seq

$T_{reg}$ cells were fixed for 10 min at 25 °C with 10% formaldehyde. After incubation, glycine was added to a final concentration of 0.125 M to `quench' the formaldehyde. Cells were pelleted, washed twice with ice-cold PBS and lysed. The lysates were pelleted, re-suspended and sonicated to reduce DNA length to 300–500 base pairs (bp). The chromatin prepared from $T_{reg}$ cells of C57BL/6 mice was incubated with protein-A-anti-Foxo1 (ab39670, Abcam) or an iso-type control antibody overnight. The chromatin prepared from $T_{reg}$ cells of *Foxo1*$^{tag/tag}$*birA Foxp3-IRES-RFP* or control *birA* mice was incubated with streptavidin overnight. The immune complexes were washed, and eluted in 500 ml of elution buffer containing 50 μM Tris, 10 mM EDTA and 1.0% SDS. Precipitated ChIP DNA and input DNA were incubated at 65 °C to reverse the crosslinking. After digestion with RNase and

proteinase K, the ChIP and input DNA were purified with phenol/chloroform extraction and ethanol precipitation. The purified DNA was repaired, ligated with an adaptor, and amplified by PCR for 15–20 cycles. The amplified DNA was purified by gel extraction and used for sequencing. SR-36 sequencing was done at the Genome Center of Cold Spring Harbor Laboratory.

### Visualizing read densities and identifying binding sites

Uniquely mapped sequence reads (36 bp) were aligned to the mouse genome (July 2007, NCBI37/mm9) using the Bowtie[33] short-read alignment software (version 0.12.7). Candidate binding sites were predicted using the MACS[34] peak detection software (version 1.4.1). In brief, MACS determines regions of enrichment by building sequencing-density profiles for sense and antisense reads, with respect to the reference, and pairing them such that the average distance between pairings can be used to model the approximate library fragment length ($d$). Reads from both strands were then repositioned by shifting a distance half the estimated fragment length, ½$d$, downstream to capture the most likely binding location at the fragment midpoint rather than skewing to the 5′ or 3′ ends. Enrichment was then determined by scanning the shifted, genome-wide read profile with a window twice the size of the estimated fragment length, where the number of shifted reads falling within this 2 × $d$ window was assumed to follow a Poisson distribution, with a mean parameter determined from the local background in the input sample. The empirical false-discovery rate (eFDR) was fine-tuned using the noise ratio to maximize the effectiveness of the peak-calling strategy. The noise ratio was defined as the number control IgG peaks overlapping control BirA peaks (control overlaps) divided by the number of Foxo1 antibody peaks overlapping Foxo1 biotin peaks (ChIP overlaps). A noise ratio threshold of 0.005 was chosen as it corresponded to a large reduction in noise. To achieve this ratio, peak-calling was performed at an eFDR of 0.01. As defined in ref. 34, false background peaks were enumerated as the number of peaks called when swapping the input and ChIP sample. The eFDR was then calculated as the number of peaks detected divided by the number of background peaks detected. We, thus, determined a suitable threshold of $P < 2.5 \times 10^{-9}$ and $P < 5.0 \times 10^{-6}$, yielding 19,904 and 61,180 significantly enriched loci for antibody- and biotin-based ChIP-seq of Foxo1, respectively. To visualize read-density profiles, we aggregated counts at each genomic position for uniquely mapped reads that were extended to the estimate $d$. Counts were then smoothed with a moving average within a 200-bp sliding window across the genome. Smoothed average counts were visualized near to genes of interest using the R software package (http://www.R-project.org).

### Associating peaks with gene features

To further refine our enriched loci, we corroborated peaks detected in antibody-based ChIP-seq with those from our biotinylated-Foxo1 tag-based method. To accomplish this, we distinguished high-confidence peaks by selecting for all `antibody' peaks overlapped by one or more `biotin' peaks and extending the 3′ and 5′ most coordinates to encompass all overlaps, so as to reduce any redundancies. The merged coordinates yielded 3,431 high-confidence, unique, merged regions, which we deemed putative Foxo1 binding sites. To associate peaks with functional regions at high precision and resolution, we intersected antibody peak summits (position of highest read density within a candidate peak region) falling within high-confidence corroborated regions with the set of genomic features (for example, 5′ UTR, 3′ UTR, exons, introns, 5-kilobase promoter, intergenic space) obtained from the UCSC Table Browser[35] (http://genome.ucsc.edu/). We also compared our regions with conserved phastCons scores and elements (Euarchontoglire subset)[36]. Over-representation of these features was estimated empirically by generating 1,000 background sets each containing 3,431 random peaks, maintaining the same distribution of chromosomes and widths as our high-confidence set. Peaks from each background set were assigned to

appropriate functional categories. The significance of the observed number of each annotation from our high-confidence summits was then inferred using a *Z*-test with respect to these randomly generated background counts.

### DNA motif analysis

We first extracted nucleotide sequences±250 bp flanking all antibody-based ChIP-seq summits associated with peaks corroborated by biotinylated-Foxo1 tag-based ChIP-seq enrichment. These DNA sequences were screened for over-representation of known consensus motifs, using both the JASPAR[37] and TRANSFAC[38] databases, and the most enriched known motifs were noted. To examine to what extent the consensus Foxo1 TRANSFAC motifs, M00473 and M00474 were enriched, we ranked our putative binding site candidates by *P* value and assessed the cumulative occurrence rate one peak at a time, from most to least enriched. This was done to illustrate the expectation that the cumulative motif occurrence rate approaches the number of peaks with a motif divided by the total number of peaks but would be significantly increased in more enriched subset of binding candidates. Occurrence was determined using the STORM motif analysis tool available in the CREAD software package[39] at a threshold of $P<1\times10^{-4}$. We further substantiated the over-representation of consensus Foxo1 motifs by performing *de novo* motif prediction from the top 500 ranked candidate binding site sequences using the GADEM[40] motif-discovery algorithm, compared to shuffled sequences with similar di-nucleotide composition as background. Statistical similarity of predicted *de novo* motifs was estimated using the Tomtom[41] motif comparison software available as part of the MEME software suite.

### Gene-expression profiling

$T_{reg}$ cells were isolated from the spleens and peripheral lymph nodes of *Foxp3*$^{cre}$*Foxo1*$^{fl/fl}$, *Foxp3*$^{cre}$*Foxo1*$^{AAA/+}$, *Foxp3*$^{cre}$*Foxo1*$^{fl/fl}$ *Foxo1*$^{AAA/+}$ and wild-type mice by FACS. RNA was prepared with the miRNeasy Mini Kit according to the manufacturer's instructions (Qiagen). Two rounds of RNA amplification, labelling and hybridization to M430 2.0 chips (Affymetrix) were done at the Core Facility of Memorial Sloan-Kettering Cancer Center.

### Microarray data analysis

Microarray data was analysed using the R statistical software package. To reduce technical variations from array to array, chip normalization was performed using robust multi-array analysis available via the affy BioConductor package and differential gene expression defined by 1.5-fold change with a false-discovery rate of <0.01 was determined using the *limma* package[42,43]. When multiple probes for a given gene were significantly differentially expressed, their $\log_2$-fold changes were averaged.

### qPCR

mRNA amounts of *Ifng, Il2ra, Ctla4* and *Actb* were determined by qPCR with the following primers: *Ifng*, 5′-gcgtcattgaatcacacctg-3′ and 5′-tgagctcattgaatgcttgg-3′; *Il2ra*, 5′-gagacttcctgccccataac-3′ and 5′-gccactgctaccttatactcc-3′; *Ctla4*, 5′-tggactccggaggtacaaag-3′ and 5′-aaacggcctttcagttgatg-3′; *Actb*, 5′-ttgctgacaggatgcagaag-3′ and 5′-acatctgctggaaggtggac-3′. The mRNA amounts were normalized to those of *Actb*. Chromatin amounts of the Foxo1 binding site in the *Ifng* locus were determined by qPCR with the following primers: 5′-gacctgcacttctgtgagca-3′ and 5′-tctccttcctgtggatcacc-3′.

### Heat-map

To effectively visualize Foxo1-dependent gene expression, we gated relative expression values on wild-type versus *Foxp3*$^{cre}$*Foxo1*$^{AAA/+}$ values; that is, the $\log_2$-fold change between wild-type versus *Foxp3*$^{cre}$*Foxo1*$^{AAA/+}$ was used to define a wild-type value equal

to½log$_2$-fold-change and a *Foxp3*$^{cre}$*Foxo1*$^{AAA/+}$ value equal to ½ log$_2$-fold change. The remaining *Foxp3*$^{cre}$*Foxo1*$^{fl/fl}$ and *Foxp3*$^{cre}$*Foxo1*$^{fl/fl}$/*Foxp3*$^{cre}$*Foxo1*$^{AAA/+}$ fold-change values were then similarly normalized with respect to this new wild-type value. We focused on the range of genes within±2 log$_2$-fold change; values exceeding this range at the extremes were coloured blue or yellow. A selection of genes was depicted in which the *Foxp3*$^{cre}$*Foxo1*$^{fl/fl}$ phenotype was partially or completely rescued by *Foxp3*$^{cre}$*Foxo1*$^{AAA/+}$, and putative Foxo1 binding sites, as determined by ChIP-seq experiments, resided nearby.

### Gene-set enrichment analysis

Gene set and pathway analysis was performed using the FatiGO[44] tool via the Babelomics[25] software suite (http://babelomics.bioinfo.cipf.es) on Foxo1-bound target genes showing differential gene expression rescued by *Foxp3*$^{cre}$*Foxo1*$^{AAA/+}$. Significantly over-represented categories were defined by an adjusted *P* value of 0.05 or less. We highlighted a selection of Gene Ontology categories and BioCarta pathways made available on the Babelomics web-based tool in our analysis.

### Statistical analysis

Student's *t*-test was used to calculate statistical significance for difference in a particular measurement between groups. A *P* value of <0.05 was considered statistically significant.

## Supplementary Material

Refer to Web version on PubMed Central for supplementary material.

## Acknowledgments

We thank R. Flavell for the Foxp3-IRES-RFP mouse strain, K. Rajewsky and C. Xiao for the *Rosa26* targeting vector and T. Unterman for the HA-hFoxo1(AAA) construct. This work was supported by the Starr Cancer Consortium (13-A123 to M.O.L., M.Q.Z. and G.A.), the Rita Allen Foundation (M.O.L.), National Bio Resource Project (NBRPC) (2012CB316503 to M.Q.Z.) and National Institutes of Health (HG001696 to M.Q.Z.).

## References

1. Sakaguchi S, Yamaguchi T, Nomura T, Ono M. Regulatory T cells and immune tolerance. Cell. 2008; 133:775–787. [PubMed: 18510923]
2. Tang Q, Bluestone JA. The Foxp3$^+$ regulatory T cell: a jack of all trades, master of regulation. Nature Immunol. 2008; 9:239–244. [PubMed: 18285775]
3. Feuerer M, Hill JA, Mathis D, Benoist C. Foxp3$^+$ regulatory T cells: differentiation, specification, subphenotypes. Nature Immunol. 2009; 10:689–695. [PubMed: 19536194]
4. Shevach EM. Mechanisms of foxp3$^+$ T regulatory cell-mediated suppression. Immunity. 2009; 30:636–645. [PubMed: 19464986]
5. Rudensky AY. Regulatory T cells and Foxp3. Immunol. Rev. 2011; 241:260–268. [PubMed: 21488902]
6. Haxhinasto S, Mathis D, Benoist C. The AKT–mTOR axis regulates *de novo* differentiation of CD4$^+$Foxp3$^+$ cells. J. Exp. Med. 2008; 205:565–574. [PubMed: 18283119]
7. Sauer S, et al. T cell receptor signaling controls Foxp3 expression via PI3K, Akt, and mTOR. Proc. Natl Acad. Sci. USA. 2008; 105:7797–7802. [PubMed: 18509048]
8. Ouyang W, et al. Foxo proteins cooperatively control the differentiation of Foxp3$^+$ regulatory T cells. Nature Immunol. 2010; 11:618–627. [PubMed: 20467422]
9. Harada Y, et al. Transcription factors Foxo3a and Foxo1 couple the E3 ligase Cbl-b to the induction of Foxp3 expression in induced regulatory T cells. J. Exp. Med. 2010; 207:1381–1391. [PubMed: 20439537]

10. Kerdiles YM, et al. Foxo transcription factors control regulatory T cell development and function. Immunity. 2010; 33:890–904. [PubMed: 21167754]
11. Ouyang W, Beckett O, Flavell RA, Li MO. An essential role of the forkhead-box transcription factor Foxo1 in control of T cell homeostasis and tolerance. Immunity. 2009; 30:358–371. [PubMed: 19285438]
12. Kerdiles YM, et al. Foxo1 links homing and survival of naive T cells by regulating L-selectin, CCR7 and interleukin 7 receptor. Nature Immunol. 2009; 10:176–184. [PubMed: 19136962]
13. Patterson SJ, et al. Cutting edge: PHLPPregulates the development, function, and molecular signaling pathways of regulatory T cells. J. Immunol. 2011; 186:5533–5537. [PubMed: 21498666]
14. Rubtsov YP, et al. Regulatory T cell-derived interleukin-10 limits inflammation at environmental interfaces. Immunity. 2008; 28:546–558. [PubMed: 18387831]
15. Kim JM, Rasmussen JP, Rudensky AY. Regulatory T cells prevent catastrophic autoimmunity throughout the lifespan of mice. Nature Immunol. 2007; 8:191–197. [PubMed: 17136045]
16. Lahl K, et al. Selective depletion of Foxp3$^{+}$ regulatory T cells induces a scurfy-like disease. J. Exp. Med. 2007; 204:57–63. [PubMed: 17200412]
17. Zhao Y, et al. Cytosolic FoxO1 is essential for the induction of autophagy and tumour suppressor activity. Nature Cell Biol. 2010; 12:665–675. [PubMed: 20543840]
18. Zhang X, et al. Phosphorylation of serine 256 suppresses transactivation by FKHR (FOXO1) by multiple mechanisms. Direct and indirect effects on nuclear/cytoplasmic shuttling and DNA binding. J. Biol. Chem. 2002; 277:45276–45284. [PubMed: 12228231]
19. Sandri M, et al. Foxo transcription factors induce the atrophy-related ubiquitin ligase atrogin-1 and cause skeletal muscle atrophy. Cell. 2004; 117:399–412. [PubMed: 15109499]
20. Gilley J, Coffer PJ, Ham J. FOXO transcription factors directly activate bim gene expression and promote apoptosis in sympathetic neurons. J. Cell Biol. 2003; 162:613–622. [PubMed: 12913110]
21. Zheng Y, et al. Genome-wide analysis of Foxp3 target genes in developing and mature regulatory T cells. Nature. 2007; 445:936–940. [PubMed: 17237761]
22. Marson A, et al. Foxp3 occupancy and regulation of key target genes during T-cell stimulation. Nature. 2007; 445:931–935. [PubMed: 17237765]
23. Gavin MA, et al. Foxp3-dependent programme of regulatory T-cell differentiation. Nature. 2007; 445:771–775. [PubMed: 17220874]
24. Wing K, et al. CTLA-4 control over Foxp3$^{+}$ regulatory T cell function. Science. 2008; 322:271–275. [PubMed: 18845758]
25. Medina I, et al. Babelomics: an integrative platform for the analysis of transcriptomics, proteomics and genomic data with advanced functional profiling. Nucleic Acids Res. 2010; 38:W210–W213. [PubMed: 20478823]
26. Hatton RD, et al. A distal conserved sequence element controls *Ifng* gene expression by T cells and NK cells. Immunity. 2006; 25:717–729. [PubMed: 17070076]
27. Crellin NK, Garcia RV, Levings MK. Altered activation of AKT is required for the suppressive function of human CD4$^{+}$CD25$^{+}$ T regulatory cells. Blood. 2007; 109:2014–2022. [PubMed: 17062729]
28. Oldenhove G, et al. Decrease of Foxp3$^{+}$ Treg cell number and acquisition of effector cell phenotype during lethal infection. Immunity. 2009; 31:772–786. [PubMed: 19896394]
29. Dominguez-Villar M, Baecher-Allan CM, Hafler DA. Identification of T helper type 1-like, Foxp3$^{+}$ regulatory T cells in human autoimmune disease. Nature Med. 2011; 17:673–675. [PubMed: 21540856]
30. McClymont SA, et al. Plasticity of human regulatoryT cells in healthy subjects and patients with type 1 diabetes. J. Immunol. 2011; 186:3918–3926. [PubMed: 21368230]
31. Wan YY, Flavell RA. Identifying Foxp3-expressing suppressor T cells with a bicistronic reporter. Proc. Natl Acad. Sci. USA. 2005; 102:5126–5131. [PubMed: 15795373]
32. Driegen S, et al. A generic tool for biotinylation of tagged proteins in transgenic mice. Transgenic Res. 2005; 14:477–482. [PubMed: 16201414]
33. Langmead B, Trapnell C, Pop M, Salzberg SL. Ultrafast and memory-efficient alignment of short DNA sequences to the human genome. Genome Biol. 2009; 10:R25. [PubMed: 19261174]

34. Zhang Y, et al. Model-based analysis of ChIP-Seq (MACS). Genome Biol. 2008; 9:R137. [PubMed: 18798982]

35. Karolchik D, et al. The UCSC Table Browser data retrieval tool. Nucleic Acids Res. 2004; 32:D493–D496. [PubMed: 14681465]

36. Siepel A, et al. Evolutionarily conserved elements in vertebrate, insect, worm, and yeast genomes. Genome Res. 2005; 15:1034–1050. [PubMed: 16024819]

37. Portales-Casamar E, et al. JASPAR 2010: the greatly expanded open-access database of transcription factor binding profiles. Nucleic Acids Res. 2010; 38:D105–D110. [PubMed: 19906716]

38. Matys V, et al. TRANSFAC: transcriptional regulation, from patterns to profiles. Nucleic Acids Res. 2003; 31:374–378. [PubMed: 12520026]

39. Smith AD, Sumazin P, Xuan Z, Zhang MQ. DNA motifs in human and mouse proximal promoters predict tissue-specific expression. Proc. Natl Acad. Sci. USA. 2006; 103:6275–6280. [PubMed: 16606849]

40. Li L. GADEM: a genetic algorithm guided formation of spaced dyads coupled with an EM algorithm for motif discovery. J. Comput. Biol. 2009; 16:317–329. [PubMed: 19193149]

41. Gupta S, Stamatoyannopoulos JA, Bailey TL, Noble WS. Quantifying similarity between motifs. Genome Biol. 2007; 8:R24. [PubMed: 17324271]

42. Irizarry RA, et al. Summaries of Affymetrix GeneChip probe level data. Nucleic Acids Res. 2003; 31:e15. [PubMed: 12582260]

43. López-Romero P. Pre-processing and differential expression analysis of Agilent microRNA arrays using the AgiMicroRna Bioconductor library. BMC Genomics. 2011; 12:64. [PubMed: 21269452]

44. Al-Shahrour F, Diaz-Uriarte R, Dopazo J. FatiGO: a web tool for finding significant associations of Gene Ontology terms with groups of genes. Bioinformatics. 2004; 20:578–580. [PubMed: 14990455]

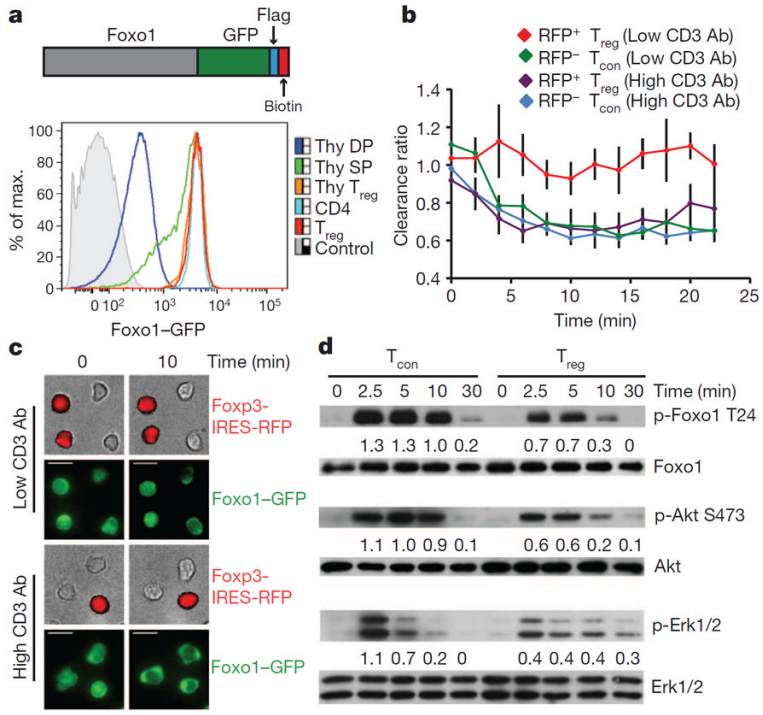


**Figure 1. Foxo1 expression and TCR-induced Foxo1 nuclear exclusion in $T_{reg}$ cells**

**a**, Foxo1 fusion protein with a tag containing GFP, Flag and a biotin-labelling peptide (top). Flow cytometric analysis of Foxo1–GFP expression in thymic $CD4^+CD8^+$ double-positive T cells (Thy DP), $CD4^+Foxp3^-$ single-positive T cells (Thy SP) and $CD4^+Foxp3^+$ $T_{reg}$ cells (Thy $T_{reg}$), and splenic $CD4^+Foxp3^-$ conventional T cells (CD4) and $CD4^+Foxp3^+$ $T_{reg}$ cells from *Foxo1*$^{tag/tag}$ mice ($T_{reg}$) (bottom). Cells from wild-type mice were used as a control. **b**, **c**, TCR-induced Foxo1 nuclear clearance in $CD4^+RFP^-$ conventional ($T_{con}$) and $CD4^+RFP^+$ $T_{reg}$ cells from *Foxo1*$^{tag/tag}$ mice. Cells were stimulated with 0.01 μg ml$^{-1}$ (low) or 0.1 μg ml$^{-1}$ (high) anti-CD3 antibody (Ab) in the presence of 1.0 μg ml$^{-1}$ anti-CD28. **b**, Quantification of Foxo1 nuclear clearance. Nuclear exclusion leads to a decrease in clearance ratio. **c**, Representative images of Foxo1 nuclear clearance of $T_{con}$ and $T_{reg}$ cells. **d**, Phosphorylated (p)-Foxo1 Thr 24, total Foxo1, p-Akt Ser 473, total Akt, p-Erk1/2 and total Erk1/2 proteins in $T_{con}$ and $T_{con}$ cells stimulated with low anti-CD3 and anti-CD28 were determined by immunoblotting. The relative amounts of p-Foxo1, p-Akt and p-Erk1/2 proteins normalized to total Foxo1, Akt and Erk1/2 proteins are shown. Error bars represent s.d.; all experiments were repeated at least three times with similar results.

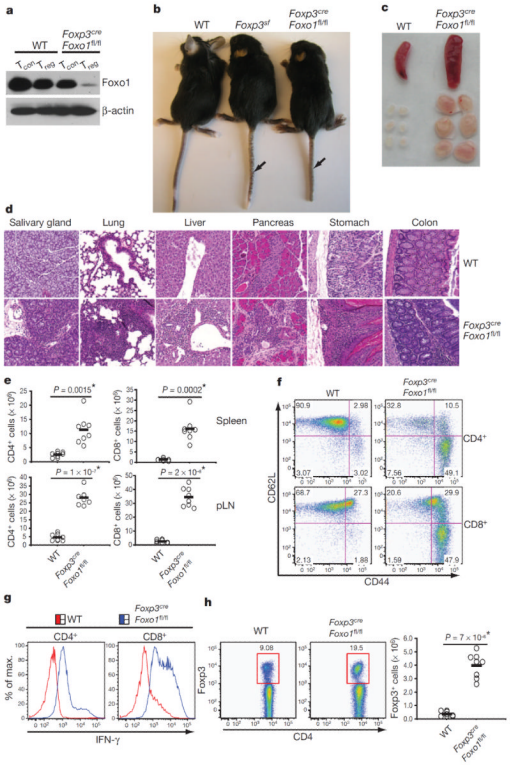


**Figure 2. An essential role for Foxo1 in the control of $T_{reg}$ cell function**

**a**, Foxo1 protein in $CD4^+Foxp3^-$ conventional ($T_{con}$) and $T_{reg}$ cells from wild-type (WT) and *Foxp3*$^{cre}$*Foxo1*$^{fl/fl}$ mice was determined by immunoblotting. β-actin was used as a loading control. **b**, Images of 21-day-old wild-type, *Foxp3*$^{sf}$ and *Foxp3*$^{cre}$*Foxo1*$^{fl/fl}$ mice. Arrows indicate the scurfy tails of *Foxp3*$^{sf}$ and *Foxp3*$^{cre}$*Foxo1*$^{fl/fl}$ mice. **c**, A representative picture of spleens and peripheral lymph nodes from 20-day-old wild-type and *Foxp3*$^{cre}$*Foxo1*$^{fl/fl}$ mice. **d**, Haematoxylin and eosin staining of salivary gland, lung, liver, pancreas, stomach and colon sections from 21-day-old wild-type and *Foxp3*$^{cre}$*Foxo1*$^{fl/fl}$ mice. **e**, $CD4^+$ and $CD8^+$ T-cell numbers from spleens and peripheral lymph nodes (pLN) of 17–21-day-old wild-type and *Foxp3*$^{cre}$*Foxo1*$^{fl/fl}$ mice ($n$=8 per genotype). **f**, Flow cytometric analysis of CD44 and CD62L expression in peripheral lymph node $CD4^+$ and $CD8^+$ T cells from 20-day-old wild-type and *Foxp3*$^{cre}$*Foxo1*$^{fl/fl}$ mice. **g**, Peripheral lymph node T cells from 20-day-old wild-type and *Foxp3*$^{cre}$*Foxo1*$^{fl/fl}$ mice were stimulated with phorbol myristate acetate (PMA) and ionomycin for 4 h. The expression of IFN-γ in $CD4^+$ and $CD8^+$ T cells was determined by intracellular staining. **h**, Flow cytometric analysis of Foxp3 expression in peripheral lymph node $CD4^+$ T cells from 20-day-old wild-type and *Foxp3*$^{cre}$*Foxo1*$^{fl/fl}$ mice (left). Peripheral lymph node $T_{reg}$ cell numbers from 17–21-day-old wild-type and *Foxp3*$^{cre}$*Foxo1*$^{fl/fl}$ mice (right; $n$=8 per genotype). The $P$ values between the two groups are shown. Asterisk indicates a statistically significant difference. Results represent at least three independent experiments.

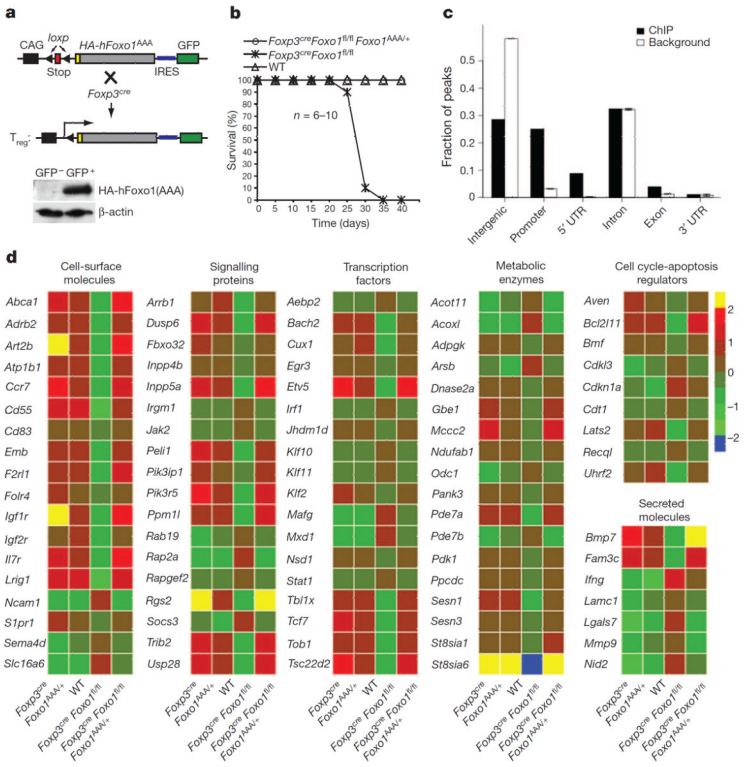


**Figure 3. Foxo1-dependent transcriptional programs in $T_{reg}$ cells**

**a**, A schematic representation of the mouse line expressing HA-hFoxo1(AAA) specifically in $T_{reg}$ cells. A cassette containing a floxed stop sequence, a cDNA coding for a HA-tagged human Foxo1(AAA) mutant, and IRES-GFP proteins was inserted into the *Rosa26* locus. Mice with the knock-in allele were crossed with *Foxp3*$^{cre}$ mice (top). The expression of HA-FOXO1(AAA) was determined by immunoblotting with anti-HA. β-actin was used as a loading control (bottom). **b**, Survival of wild-type, *Foxp3*$^{cre}$*Foxo1*$^{fl/fl}$ and *Foxp3*$^{cre}$*Foxo1*$^{fl/fl}$*Foxo1*$^{AAA/+}$ mice ($n$=6 to 10 per genotype). **c**, The overlapping set of peaks shared between antibody and biotin ChIP-seq samples was associated with functional annotations based on the genomic location of the summits within each peak, which revealed enrichment in gene promoters ($P$=0.04) and 5′ UTRs ($P<1\times10^{-10}$) above the background rate using randomly generated peaks. **d**, Foxo1-bound target genes differentially expressed between wild-type and *Foxp3*$^{cre}$*Foxo1*$^{fl/fl}$ $T_{reg}$ cells, and whose expression was corrected in *Foxp3*$^{cre}$*Foxo1*$^{fl/fl}$*Foxo1*$^{AAA/+}$ $T_{reg}$ cells.

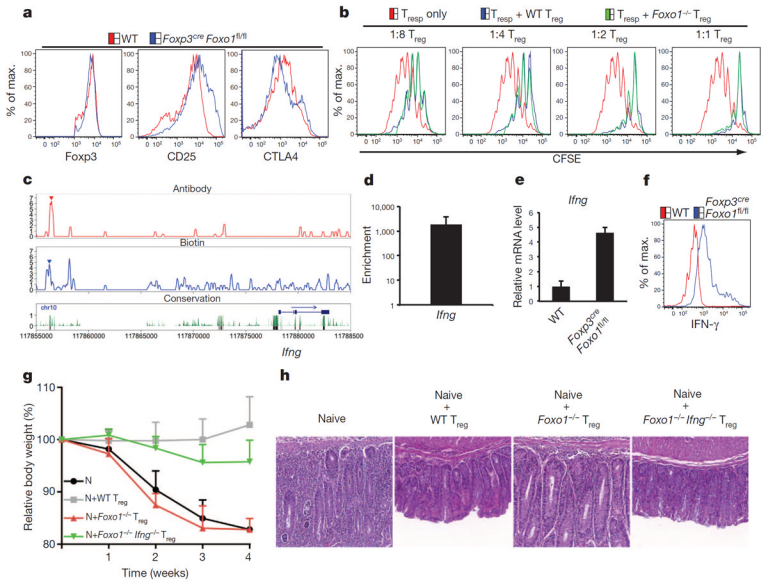


**Figure 4. Restoration of Foxo1-deficient $T_{reg}$ cell function in the absence of IFN-γ**

**a**, Flow cytometric analysis of Foxp3, CD25 and CTLA4 expression in lymph node $T_{reg}$ cells from 20-day-old wild-type and *Foxp3*$^{cre}$*Foxo1*$^{fl/fl}$ mice. **b**, Suppression of wild-type naive CD4$^{+}$ T cells, labelled with the cytosolic dye carboxyfluorescein diacetate succinimidyl ester (CFSE) (responding T cells ($T_{resp}$)), by wild-type and Foxo1-deficient (Foxo1$^{-/-}$) $T_{reg}$ cells. $T_{resp}$ cell division was assessed by CFSE dilution at the indicated ratios of cell numbers between $T_{reg}$ cell and $T_{resp}$ cells. **c**, Foxo1-bound regions in the *Ifng* locus. **d**, Foxo1 binding to the ChIP-seq peak was confirmed by ChIP-quantitative (q)PCR, and is presented relative to enrichment by immunoprecipitation with isotype-matched control antibody. **e**, Expression of IFN-γ mRNA in $T_{reg}$ cells from wild-type and *Foxp3*$^{cre}$*Foxo1*$^{fl/fl}$ mice was determined by qPCR. **f**, Peripheral lymph node T cells from 20-day-old wild-type and *Foxp3*$^{cre}$*Foxo1*$^{fl/fl}$ mice were stimulated with PMA and ionomycin for 4 h. The expression of IFN-γ in $T_{reg}$ cells was determined by intracellular staining. **g**, **h**, Naive T cells (N) were transferred to *Rag1*$^{-/-}$ mice alone or in combination with wild-type, *Foxo1*$^{-/-}$ or *Foxo1*$^{-/-}$ *Ifng*$^{-/-}$ $T_{reg}$ cells. Changes in body weight of *Rag1*$^{-/-}$ recipients over time are shown ($n$=4) (**g**). Haematoxylin and eosin staining of colon sections from *Rag1*$^{-/-}$ mice at 4 weeks after the transfer (**h**). Error bars represent s.d.; results are representative of at least three independent experiments.